PHYSICAL REVIEW B VOLUME 49, NUMBER 11 15 MARCH 1994-I

Optical properties of zinc-blende CdSe and $Zn_xCd_{1-x}Se$ films grown on GaAs

Y. D. Kim, M. V. Klein, S. F. Ren, and Y. C. Chang
*Department of Physics and Materials Research Laboratory, University of Illinois at Urbana-Champaign,
1110 West Green Street, Urbana, Illinois 61801*

H. Luo, N. Samarth,* and J. K. Furdyna
Department of Physics, Room 225, University of Notre Dame, Nieuwland Science Hall, Notre Dame, Indiana 46556

(Received 21 May 1993; revised manuscript received 18 October 1993)

We present room-temperature ellipsometric measurements of the dielectric function of $Zn_xCd_{1-x}Se$ single-crystal films grown on (001)GaAs in the 1.5–6.0-eV energy region x ranging from 0 to 1. We identify the E_0, $E_0+\Delta_0$, E_1, $E_1+\Delta_1$, and E_2 threshold energies using the CdSe band structure calculated with a nonlocal empirical pseudopotential method. We find that the contact exciton effect has to be included in the calculated dielectric function of CdSe in order to obtain good agreement with our measurements. A compositon-dependent critical-point analysis of the E_1 and $E_1+\Delta_1$ structures has been performed. We also find that the spin-orbit-splitting band gap $\Delta_1(x)$, the linewidths, and the excitonic angles are about maximum at $x=0.5$, which we attribute to the statistical fluctuation of the alloy composition. Finally, the E_1 and $E_1+\Delta_1$ critical-point amplitudes cannot be understood by the one-electron approximation, confirming the existence of strong excitonic effects.

I. INTRODUCTION

Bulk cadmium selenide is a prototype of a hexagonal wurtzite semiconductor,[1] and its optical properties[2–12] and band structure have been extensively studied.[13–15] However, after the discovery of blue-green lasing action in (Zn,Cd)Se/ZnSe systems,[16–18] additional study of the optical properties of zinc-blende CdSe and $Zn_xCd_{1-x}Se$ alloys became necessary. The study of the optical properties of semiconducting alloys is very useful in analyzing band-structure changes from one semiconductor to another. The properties at energies greater than those of the fundamental band gap E_0 are of particular interest, since the structure in the optical spectra can be assigned to direct electronic transitions at specific regions of the Brillouin zone (BZ) and therefore can be related to the band structure of the semiconductor alloys.

While several ellipsometric studies on hexagonal CdSe have been reported,[19–21] to our knowledge no ellipsometric study has yet been reported on zinc-blende CdSe or $Zn_xCd_{1-x}Se$. The change in the fundamental gap of $Zn_xCd_{1-x}Se$ with composition has been investigated with reflection spectroscopy.[22] Heterojunctions of $ZnSe/Zn_xCd_{1-x}Se$ have also been the object of investigations.[22–24] Alloying studies show that the fundamental gaps of semiconductors scale quadratically with composition x. This "bowing" of E_0 with x is believed to make two contributions.[25] One is the difference in the lattice constants among the various constituents in the virtual-crystal approximation (VCA), and the other is the effect of the random potential due to disorder. For higher band gaps the magnitude and even the sign of the bowing relative to the fundamental edge can change.[26] Lifetime broadening effects due to alloying are also present in higher band gaps,[27] as is a nonlinear dependence of spin-orbit (SO) splitting on alloy composition induced by disorder.[28,29]

In this work we present an ellipsometric study at room temperature of zinc-blende $Zn_xCd_{1-x}Se$ alloys ($0\le x\le 1$) in the energy range from the near-infrared (1.5 eV) to the near-ultraviolet (6.0 eV) and we also present a band-structure calculation of zinc-blende CdSe. Automatic spectroscopic ellipsometry is an excellent technique for investigating the optical response of semiconductors[30] and has been used to study Si (Refs. 31 and 32) and Ge,[31,33] as well as III-V (Refs. 31 and 34–41) and II-VI (Refs. 19 and 42–47) compound semiconductors and their alloys. Analysis of the numerical second derivative spectra of the complex dielectric constant with respect to the photon energy $d^2\varepsilon/d\omega^2$ allows an accurate determination of the energy threshold (E), linewidth (Γ), and phase (ϕ) of the critical points (CP's). We found a quadratic dependence of E_1 and $E_1+\Delta_1$ band-gap energies on composition x. An increase of the linewidth of the alloys with respect to the parent compounds was observed, reaching its maximum at the concentration $x\sim 0.5$.

Section II describes the sample preparation, the experimental technique, and the chemical treatment. In Sec. III A the dielectric functions of CdSe and its band structure are presented. Section III B assesses the composition-dependent dielectric functions of $Zn_xCd_{1-x}Se$ alloys and their CP parameters.

II. EXPERIMENTAL DETAILS

In the bulk, a single crystal of the $Zn_xCd_{1-x}Se$ alloy has the zinc-blende structure for $x\le 0.3$, the hexagonal wurtzite structure for $x\ge 0.5$, and mixed phases for $0.3<x<0.5$.[48] In contrast, we found that the heteroepitaxy of $Zn_xCd_{1-x}Se$ on (100)GaAs by molecular-beam

0163-1829/94/49(11)/7262(9)/$06.00

epitaxy (MBE) results in single-phase zinc-blende crystals over the entire composition range from ZnSe to CdSe. In this work, all $Zn_xCd_{1-x}Se$ layers were grown on GaAs except the pure CdSe film, which was grown on a buffer layer of ZnTe on GaAs. Crystal growth was carried out in a Riber 32 R&D system, with elemental sources of Zn and Se, and either Cd or compound CdSe sources. The composition of the alloy samples was determined by assuming a linear variation of the lattice constant (Vegard's law), and also confirmed by energy-dispersive x-ray fluorescence analysis. The thickness of the layers was over 1 μm. Details about the growth conditions and the characterizations are described in Refs. 22, 23, 49, and 50.

Dielectric function spectra $\langle \varepsilon(\omega) \rangle = \langle \varepsilon_1(\omega) \rangle + i \langle \varepsilon_2(\omega) \rangle$ were measured at room temperature between 1.5 and 6.0 eV using an automatic spectroscopic rotating analyzer ellipsometer of the type developed by Aspnes.[51,52] Light from a 75-W xenon lamp was dispersed by a Cary 14R monochromator, and then linearly polarized with a Rochon-quartz prism. Upon reflection from the sample the linearly polarized light becomes elliptically polarized. The reflected light is modulated by means of a rotating analyzer (Rochon prism) and detected by a photomultiplier. The output of the photomultiplier is digitized, and the signal is analyzed with the aid of a personal computer. The measurements were generally performed at an incident angle of 68.4°.

The sample was mounted and optically aligned with a He-Ne laser in a windowless cell in flowing purified N_2 to minimize surface contamination. It is well known that the existence of overlayers on the surface complicates efforts to obtain the intrinsic dielectric response of the sample by ellipsometry because of its surface sensitivity.[31] Therefore, the samples have to be etched *in situ* immediately before the measurement. We followed that wet chemical etching procedure described in Ref. 47, where the successful removal of the oxide overlayer on ZnSe was reported. The chemical treatment was repeated until real-time ellipsometric spectra showed no more changes, and the highest values of ε_2 at the $E_1 + \Delta_1$ band-gap energy region were obtained. Figure 1 shows the real and imaginary parts of the pseudodielectric function after chemical treatment of CdSe. The pseudodielectric function $\langle \varepsilon \rangle$ is defined as the measured or apparent dielectric function obtained by reducing the ellipsometric data with the two-phase (ambient-substrate) model,[53] ignoring the presence of possible surface overlayers and microscopic roughness. After the chemical treatment of a 1:3 mixture of NH_4OH (29%): methanol, the real part of the spectrum was significantly enhanced, contrary to the case of hexagonal CdSe.[19] The difference between these two experiments may not easily be explained because the characteristics of chemical etching depend not only on the crystal orientations and the structures but also on the different chemicals used and on conditions such as temperature and the concentrations.[54] All other alloy samples were treated in the same way and showed similar behaviors.

III. RESULTS AND DISCUSSIONS

A. CdSe

The real and imaginary parts of the pseudodielectric function $\langle \varepsilon \rangle$ for zinc-blende CdSe films grown on the ZnTe buffer layer on the GaAs substrate in the 1.5–6.5-eV range are shown in Fig. 2. The large oscillations below ~1.7 eV are interference patterns from the transparent characteristics of the films below their fundamental band-gap energies, and these effects can be seen up to 2 eV, where the penetration depth of the probing light becomes much smaller than the thickness of the films. The multilayer calculation[53] to remove these interference patterns was not carried out because of the uncertainty in the thicknesses of the CdSe film and ZnTe buffer layer. However, since the thickness of the CdSe film is much larger than the critical thickness for strain relaxation, we expect the dielectric response of this film to be essentially

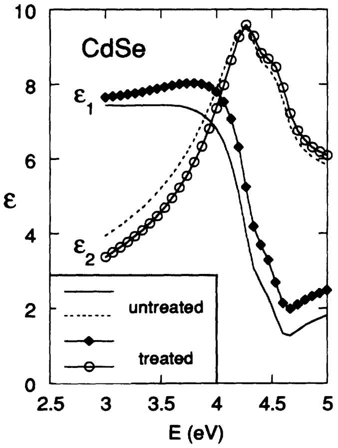

FIG. 1. Pseudodielectric function for CdSe film before (solid and dotted lines) and after (filled diamonds and open circles connected by solid lines) chemical etching of CdSe film described in Ref. 47. The enhancement of the structures is easily seen.

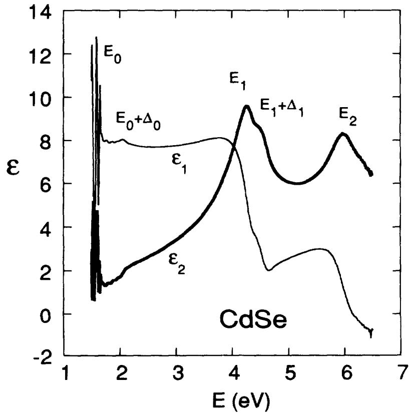

FIG. 2. Real (thin) and imaginary (thick) parts of the pseudodielectric function $\langle \varepsilon \rangle = \langle \varepsilon_1 \rangle + i \langle \varepsilon_2 \rangle$ for cubic CdSe film grown on a ZnTe buffer on a GaAs substrate. The large oscillations below the fundamental band gap are interference patterns.

that of bulk CdSe. Although the normal upper limit of our spectra range is 6 eV, the spectrum was extended to 6.5 eV to see the clear existence of a strong structure at around 6 eV. The spectra above 6 eV show considerable noise since the light intensity from the xenon lamp decreases sharply above this energy, and consequently the regulation mechanism[55] in the circuit for the photomultiplier tube fails to perform its function. Therefore the existence of structure in $\langle \varepsilon \rangle$ at 6 eV can be confirmed, but the absolute values of $\langle \varepsilon \rangle$ over 6 eV cannot be used in a quantitative analysis.

To identify the structures shown in the spectrum, we calculated the room-temperature band structure of zinc-blende CdSe by the nonlocal empirical pseudopotential method,[56] and the result is shown in Fig. 3. The empirical parameters used to fit our measured band gaps are listed in Table I. Our nonlocal potentials taken the form $V_{\mathrm{NL}}=\sum_{lm} A_l e^{-(r/R_c)^2} |lm\rangle\langle lm|$, where A_l for different angular momentum l are adjustable parameters. The core radius R_c is fixed at 2.3 a.u. The spin-orbit coupling in each material is also included empirically with the form $V_{\mathrm{SO}}=\lambda\sum_{b,b'}|b\rangle\langle b|\vec{\sigma}\cdot\vec{L}|b'\rangle\langle b'|$, where $\langle \vec{r}|b\rangle=\{x,y,z\}e^{-(r/R_c)^2}/\sqrt{S}$ denote three effective p-like core orbitals, S being the normalization constant. There are a few reports of band-structure calculations for cubic CdSe,[57,58] but we believe this is the first calculation that includes the spin-orbit-coupling effect. Several interband transitions related to CPs at different parts of the BZ are indicated. With this result, we could identify the structure in Fig. 2 as E_0, $E_0+\Delta_0$, E_1, $E_1+\Delta_1$, and E_2 threshold energies. The resulting CP transition energies obtained from the band-structure calculation are in good agreement with the experimental data, as shown in Table II. In Fig. 2, the peak at 6.0 eV is identified as the E_2 $(X_7^v \rightarrow X_6^c)$ transition, whose theoretically calculated energy is 6.069 eV. The $E_2+\Delta_2$ $(X_6^v \rightarrow X_6^c)$ transition at the X point, and the $E_2(\Sigma)$ transition which occurs along the Σ direction are also believed to contribute to this peak.

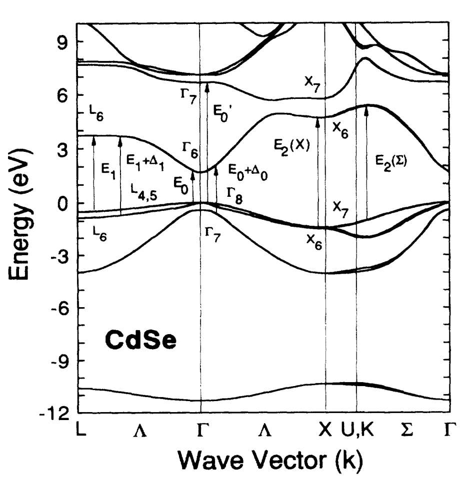

FIG. 3. Electronic energy-bandy structure of zinc-blende CdSe calculated by nonlocal empirical pseudopotential method, showing the main interband critical points.

TABLE I. Pseudopotential parameters for zinc-blende CdSe (at room temperature).

$V^S(\sqrt{3})$	$V^S(\sqrt{8})$	$V^S(\sqrt{11})$	$V^A(\sqrt{3})$	$V^A(\sqrt{4})$	$V^A(\sqrt{11})$	Lattice constant (Å)
0.277	0	0.078	0.076	0.085	0.032	6.052

Nonlocal parameters	Se	Cd
A_0	0.025	0
A_1	0	0.010
A_2	0	0.628
λ	0.000 41	0.000 19

Judging from the InP dielectric function spectrum in Ref. 37, the slight change of the slope in the real part of our spectrum at around 6.3 eV indicates the existence of another transition at higher energy, which could be a theoretically predicted E_0' transition at 6.668 eV in Table II.

Table II also includes a comparison between the critical points of hexagonal (wurtzite) and cubic (zinc-blende) CdSe. Birman[59] explained the relationship between the two structures, and their correspondences are also discussed by Bergstresser and Cohen.[13] The conduction- and valence-band edges are at the zone center (Γ point) in both zinc-blende (shown in Fig. 3) and wurtzite CdSe, making both direct-band-gap materials.[13–15] However, because of the higher symmetry of the zinc-blende structure, the slightly split $E_0(A)$ and $E_0(B)$ transition in wurtzite CdSe correspond to the degenerate E_0 transition in zinc-blende CdSe, whereas the spin-orbit-split $E_0(C)$ transition corresponds to the $E_0+\Delta_0$ transition. For zinc-blende CdSe we found that our experimental and theoretical band gap for E_0 is about 100 meV smaller than the average of the reported $E_0(A)$ and $E_0(B)$ gaps of wurtzite CdSe.[5,11,19] The spin-orbit-split $E_0+\Delta_0$ gap of this work is also about 100 meV smaller than the reported $E_0(C)$ band gap.[5,11,19] This same energy difference in band gaps between zinc-blende and wurtzite ZnS was discussed in Ref. 13. The [111] direction of zinc blende is made to correspond to the [0001] direction of the hexagonal axis, but the L point of the zinc-blende structure is mapped onto the Γ point of the hexagonal structure. Therefore $E_1(A)$ and $E_1(C)(U_4^v \rightarrow U_3^c)$ transitions in wurtzite correspond to the degenerate E_1 in zinc blende, whereas $E_1(B)$ and $E_1(C)(U_3^v \rightarrow U_3^c)$ correspond to the $E_1+\Delta_1$ transition. Comparison of the average of the split wurtzite transitions reported[5,7,12,19] with those of degenerate zinc-blende transitions observed in this work in the 4–5-eV region also gives the same tendency as at the E_0 band gap. Likewise, our zinc-blende E_2 transition is smaller than the wurtzite $E_2(K_3^v \rightarrow K_2^c)$ transition.[60] The calculated effective masses at the Γ point are also tabulated in Table III.

The calculated dielectric function from our band structure using the general formula of the one-electron picture[61] deviates significantly from the measured spectrum in Fig. 4. Thus the one-electron approximation fails adequately to explain the experiments because of its neglect

TABLE II. Calculated and experimentally obtained critical point energies (in eV) for zinc-blende CdSe in this work. Wurtzite CdSe values reported by ellipsometry study in Ref. 19 are also listed for comparison.

Zinc-blende CdSe (this work)			Wurtzite CdSe (reported in Ref. 19)	
	Calculation	Experiment		
$E_0(\Gamma_8^v \rightarrow \Gamma_6^c)$	1.666	~ 1.66	1.741	$E_0(A)(\Gamma_9^v \rightarrow \Gamma_7^c)$
			1.762	$E_0(B)(\Gamma_7^v \rightarrow \Gamma_7^c)$
$E_0+\Delta_0(\Gamma_7^v \rightarrow \Gamma_6^c)$	2.056	~ 2.05	2.167	$E_0(C)(\Gamma_7^v \rightarrow \Gamma_7^c)$
$E_1(L_{4,5}^v \rightarrow L_6^c)$	4.197	4.314	4.152	$E_1(A)(\Gamma_5^v \rightarrow \Gamma_3^c)$
			4.838	$E_1(C)(U_4^v \rightarrow U_3^c)$
$E_1+\Delta_1(L_6^v \rightarrow L_6^c)$	4.546	4.568	4.438	$E_1(B)(\Gamma_5^v \rightarrow \Gamma_3^c)$
			4.903	$E_1(C)(U_3^v \rightarrow U_3^c)$
$E_2(X_7^v \rightarrow X_6^c)$	6.069	~ 6.0	6.36[a]	$E_1(C)(U_3^v \rightarrow U_3^c)$
$E_2+\Delta_2(X_6^v \rightarrow X_6^c)$	6.149			
$E_0'(\Gamma_8^v \rightarrow \Gamma_7^c)$	6.668	≥ 6.5		

[a] This value is from Ref. 60.

of the electron-hole interaction. This tends to enhance lower-energy structures at the expense of higher-energy ones. One way to add many-body effects to the dielectric function is to utilize the Slater-Koster model,[62,63] which has been applied to many semiconductors.[36,64,65] Within this model, the Coulomb interaction is truncated beyond a certain value of the electron-hole separation. The simplest approximation is that of a Slater-Koster "contact" potential, which is set to zero except when the Wannier electron and hole are in the same unit cell. This contact interaction can be parameterized to describe the deviation of the dielectric function from the one-electron picture:[64,66]

$$\varepsilon(\omega)-1=\frac{\bar{\varepsilon}(\omega)-1}{1-g_0\hbar^2\omega^2[\bar{\varepsilon}(\omega)-1]}, \tag{1}$$

where $\bar{\varepsilon}(\omega)$ is the one-electron dielectric function, and the parameter g_0 is the strength of the contact potential. With $g_0=0.0038\ \mathrm{eV}^{-2}$, the calculated dielectric function in the 2–6-eV range agrees satisfactorily with the measured data, and the result is shown in Fig. 4. The residual deviations after this contact-potential correction are attributed to the oversimplification of the model. In the contact-potential approximation, the coupling strength between any two **k**-space states is the same, whereas in reality the coupling should be reduced with an increasing difference in wave vector. Thus the sharp decline of ε_2 at energies higher than 6 eV may be an artifact of this model.

TABLE III. Effective masses for zinc-blende CdSe at the Γ point calculated from the band structure in Fig. 3; m_{SO} is the effective mass at the spin-split valence band (Γ_7); m_{lh} and m_{hh} are light- and heavy-hole masses, respectively; m_c is the conduction-band effective mass.

Direction	m_{SO}	m_{lh}	m_{hh}	m_c
(111)	0.34	0.16	2.14	0.12
(100)	0.34	0.18	0.9	0.12
(110)	0.34	0.16	1.7	0.12

Note that although the excitonic effect significantly modifies the ε_2 spectrum, it has only a minor effect near the Γ point. The dielectric constant from Landolt-Börnstein[67] [$\varepsilon(0)\cong 10$] and the effective masses of CdSe from Table II give a binding energy for the exciton at the Γ point of $\cong 8$ meV, which is much less than k_BT at room temperature. However, since the joint density of states at the L and X critical points is much larger, the excitonic effects there are much more significant.

B. $\mathrm{Zn}_x\mathrm{Cd}_{1-x}\mathrm{Se}$ alloys

Figure 5 shows the real ($\langle\varepsilon_1\rangle$) and imaginary ($\langle\varepsilon_2\rangle$) parts of the pseudodielectric function for zinc-blende $\mathrm{Zn}_x\mathrm{Cd}_{1-x}\mathrm{Se}$ alloy films. Again the anomaly at the lowest energy region of each spectrum results from the interference patterns, and is cut arbitrarily to avoid the overlap in the spectra. The shift of four main peaks (E_0, $E_0+\Delta_0$, E_1, and $E_1+\Delta_1$) to higher energies with increasing Zn concentration x is easily seen. A decrease of the height of the ε_1 value at the E_1 peak occurs until concentrations of $x\sim 0.5$, then this feature begins to reemerge smoothly until it reaches the corresponding value for ZnSe. The same behavior is observed for ε_2 at the E_1 and

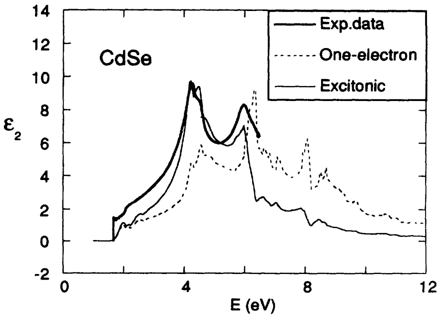

FIG. 4. Comparison of the measured (thick solid line) and calculated imaginary parts of the dielectric function for CdSe within the one-electron picture (dotted line), and with electron-hole interactions (thin solid line).

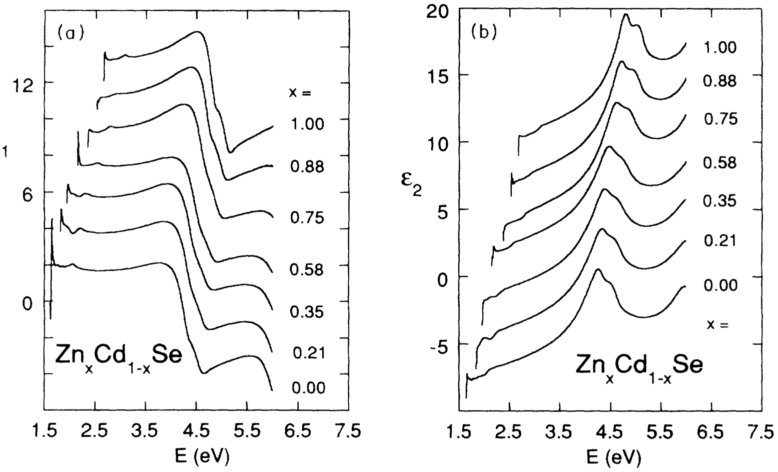

FIG. 5. (a) Real and (b) imaginary parts of the pseudodielectric function $\langle \varepsilon \rangle = \langle \varepsilon_1 \rangle + i \langle \varepsilon_2 \rangle$ of $Zn_xCd_{1-x}Se$ for several compositions. Spectra have been offset by increments of 2 and 3 relative to the center spectrum of the $x = 0.58$ sample for the real and imaginary parts, respectively.

$E_1 + \Delta_1$ structures, showing also that highly resolved peaks at $x = 1.0$ lose their sharpness at $x \sim 0.5$, and start to regain it as they approach the other end point at $x = 0.0$. The pure ZnSe ($x = 1.0$) spectrum obtained in this work has almost the same value as the one we reported earlier.[47] The main discrepancy is the slightly higher ε_1 value at E_1 which, we believe, is due to the different growth condition, and this discrepancy results in no difference in the CP parameter analysis.

1. E_0 and $E_0 + \Delta_0$ transitions

E_0 and $E_0 + \Delta_0$ represent the lowest direct gaps. Since they are localized at the Γ point of the BZ (Fig. 3), where there is a small density of states, they appear only as small peaks in the real part of the dielectric function. As was mentioned above, since the film's finite thickness results in pronounced interference patterns in this energy range, and the residual oscillations reach into the regions of $E_0 + \Delta_0$ transitions, it was impossible to carry out numerical analysis on these transitions. However, from the maxima in the real part of the dielectric function, the energies of the E_0 and $E_0 + \Delta_0$ transitions could be determined,[37] and the result are shown in Fig. 6. The $E_0(x)$ values obtained in this work show the same behavior as that reported in Ref. 22, but are shifted by about 0.09 eV to lower energies. The cause of this kind of discrepancy between ellipsometry and reflectivity measurements has been reported before.[44,68] They pointed out that the ellipsometry measurement, in general, provides more information than the reflectivity measurement since it measures phase as well as intensity.

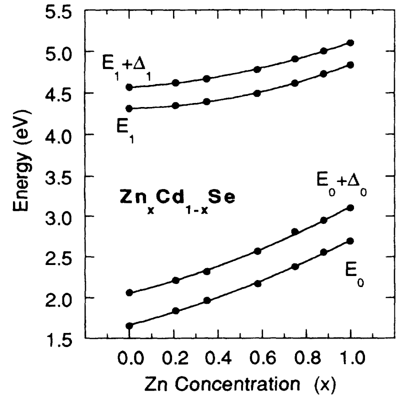

FIG. 6. Composition dependence of E_0, $E_0 + \Delta_0$, E_1, and $E_1 + \Delta_1$ energies of $Zn_xCd_{1-x}Se$. Lines represent the fits to quadratic equations of Eq. (3). Error bars are not displayed, since they are smaller than the filled circles.

2. E_1 and $E_1 + \Delta_1$ transitions

To perform a line-shape analysis of the E_1 and $E_1 + \Delta_1$ structures in our spectra, and thus to obtain the values of the CP parameters, the second derivatives of the dielectric spectra were calculated numerically.[69] An appropriate level of smoothing was also allowed in order to suppress the noise in the derivative spectra without distorting the line shape. The resulting spectra were fitted to the standard analytic critical-point (interband transition) line shape:[70,71]

$$\frac{d^2\varepsilon}{d\omega^2} = \begin{cases} n(n-1)Ae^{i\phi}(\omega - E + i\Gamma)^{n-2}, & n \neq 0 \\ Ae^{i\phi}(\omega - E + i\Gamma)^{-2}, & n = 0, \end{cases} \tag{2}$$

where a critical point is described by the amplitude A, threshold energy E, broadening Γ, and excitonic phase angle ϕ. The exponent n has the values $-\frac{1}{2}$, 0, and $\frac{1}{2}$ for one-, two- (logarithmic), and three-dimensional critical points, respectively. Discrete excitons are represented by $n = -1$. The electron-hole interaction effect on the dielectric function discussed in Sec. III A is now described as a phenomenological excitonic angle in this equation. (For the excitonic line shape, a phase angle $\phi \neq 0$ corresponds to a line shape resulting from the interaction of a discrete excitation with a continuous background.[36]) A least-squares fit procedure was used to fit the real and the imaginary parts of $d^2\varepsilon/d\omega^2$ simultaneously. The E_1 and $E_1 + \Delta_1$ transitions take place along Λ directions of the BZ (see Fig. 3). Since their longitudinal effective mass is much larger than their transverse one, these transitions are generally interpreted as two-dimensional saddle points. Hence two-dimensional CP line shapes were used for the E_1 and $E_1 + \Delta_1$ data, as in the case of hexagonal CdSe work[19] and other alloy studies,[39,43,44] and both singularities were fitted simultaneously. For ZnSe, differences in the fitted E_1 and $E_1+\Delta_1$ band-gap energies between this work and the previously reported one[47] lie within the experimental error.

In Fig. 7 we display the second-derivative spectra of $\mathrm{Zn}_x\mathrm{Cd}_{1-x}\mathrm{Se}$ together with the best fits using Eq. (2). The dots represent experimental data for $d^2\varepsilon_1/d\omega^2$. (For clarity, $d^2\varepsilon_2/d\omega^2$ are not shown, but the quality of the fits is similar.) Both E_1 and $E_1+\Delta_1$ structures are significantly enhances, and the shifts of the peaks with composition are easily seen. The fitted band-gap energies in Fig. 6 show a smooth quadratic dependence of the gaps on concentration, as in many other semiconductor alloys.[29,34,43,72–76] The solid lines correspond to the fit of our data to the expression

$$E(x)=a+bx+cx^2 . \tag{3}$$

The resulting values are listed in Table IV. The values of a obtained in this work, which are the E_1 and $E_1+\Delta_1$ band gaps of CdSe, agree well with the only reported values for zinc-blende CdSe in Ref. 60, which are also shown in parentheses in Table IV. For completeness, in Table IV we also include our estimates for the a, b, and c parameters for E_0 and $E_0+\Delta_0$, with the understanding that these may be subject to some error, as discussed in connection with Fig. 6 in Sec. III B 1.

A large nonlinearity of $\Delta_1(x)$ in this alloy was observed and is shown in Fig. 8. This deviation from the linear variation expected in the virtual-crystal approximation (VCA) was explained as being due to statistical fluctuations in the crystal potential in compositionally disordered semiconductor compounds.[25,28,29,27] The proposed Van Vechten–Berolo–Woolley (VV-B-W) model for $\Delta_1(x)$ is[77]

$$\Delta_1(x)-\Delta_{1V}(x)=\frac{x(1-x)KC_{ZC}^2}{\Delta_{1V}(x)} , \tag{4}$$

where K is a constant ($K=0.14$) which relates the strength of the model's selection rule for the fluctuating potential, and Δ_{1V} is the linear interpolation of Δ_1 (VCA). The coefficient C_{ZC} is the magnitude of the fluctuations of the actual potential in the virtual-lattice approximation:

$$C_{ZC}=be^2\left|\frac{Z_{\mathrm{Zn}}}{r_{\mathrm{Zn}}}-\frac{Z_{\mathrm{Cd}}}{r_{\mathrm{Cd}}}\right|\exp(-Rk_s) , \tag{5}$$

where b is a constant ($b=1.5$), Z and r are the valence and covalent radius of each cation element, and k_S and R are linearized Thomas-Fermi screening wave numbers for the valence electrons and covalent radius, respectively. The estimated $\Delta_1(x)$ in Eq. (4) obtained by using values in Refs. 78 and 79 is shown as a solid line in Fig. 8, and agrees well with our experimental points. Therefore, the observed nonlinearity is attributed to the effects of the random potential due to disorder.

Figure 9 displays the Lorentzian broadening parame-

TABLE IV. Values of the parameters for zinc-blende $\mathrm{Zn}_x\mathrm{Cd}_{1-x}\mathrm{Se}$ alloy obtained by fitting the critical-point energy (E), Lorentzian broadening (Γ), and the excitonic phase angle (ϕ) vs composition (x) to the quadratic equation $f(x)=a+bx+cx^2$.

	a (eV)	b (eV)	c (eV)
E_0	1.66	0.73	0.30
$E_0+\Delta_0$	2.05	0.68	0.38
E_1	4.314±0.003 (4.30)	0.055±0.018	0.467±0.016
$E_1+\Delta_1$	4.568±0.003 (4.56)	0.182±0.019	0.351±0.018
$\Gamma(E_1)$	0.092±0.001	0.176±0.007	−0.188±0.007
$\Gamma(E_1+\Delta_1)$	0.116±0.001	0.076±0.006	−0.090±0.005
$\phi(E_1)$[a]	146±5	−154±22	147±20
$\phi(E_1+\Delta_1)$	128±4	−101±20	100±19

[a] Excitonic angles are in degrees.

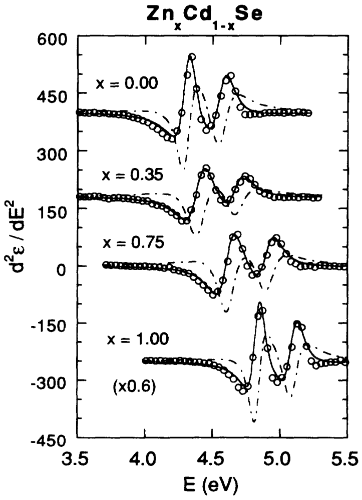

FIG. 7. Fits to the second derivatives of the real (solid) and imaginary (dashed) parts of the dielectric function of $\mathrm{Zn}_x\mathrm{Cd}_{1-x}\mathrm{Se}$. The dots represent experimental data for $d^2\varepsilon_1/d\omega^2$. To show the quality of the fits clearly, we reduced the number of data points in the graph to one-third.

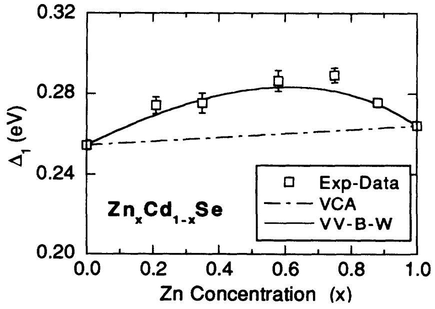

FIG. 8. Concentration-dependent spin-split band gap Δ_1. The dot-dashed line is the linear interpolation from the virtual-crystal approximation, while the solid line is estimated from Eqs. (4) and (5).

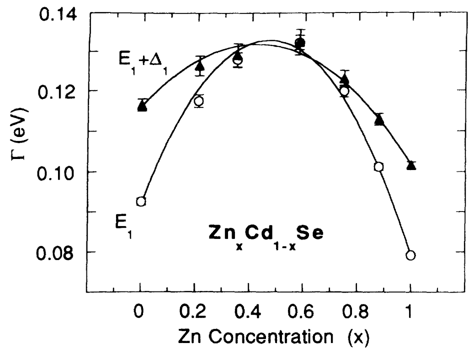

FIG. 9. Dependence of the linewidth on concentration x defined in Eq. (2) for $Zn_xCd_{1-x}Se$. Solid lines are fits to the quadratic x dependence.

ters $\Gamma(x)$ for E_1 (open circles) and $E_1+\Delta_1$ (filled triangles) CP's. Lines are the result of the fit to quadratic equations, and the fitting parameters are listed in Table IV. While other alloy systems such as $Al_xGa_{1-x}As$, $Cd_xHg_{1-x}Te$, $Zn_xCd_{1-x}S$, and CdS_xSe_{1-x} (Refs. 39, 43, and 80) show a strong asymmetry in $\Gamma(x)$, we observed symmetric behavior in this $Zn_xCd_{1-x}Se$ work. The statistical fluctuation of the alloy composition mentioned above should cause an inhomogeneous broadening of the band-gap energy which can be represented by the parabola $Cx(1-x)$.[81] The fit of our data without linear background results in $\Gamma(E_1)=0.092+0.189x-0.188x^2$ (eV) and $\Gamma(E_1+\Delta_1)=0.116+0.090x-0.090x^2$ (eV), which are exact parabolas to show the consistent behavior due to the alloying effect of random atomic potentials which we treated in the analysis of $\Delta_1(x)$.

The composition dependence of excitonic phase angle is shown in Fig. 10. The phase angle in Eq. (2) describes a metamorphism of CP line shapes due to excitonic effects by allowing a continuous admixture between adjacent CP's.[82,83] In the case of two-dimensional (2D) CP's this limits ϕ to the range 0°–270° (however, when the E_1 structure is treated as an uncorrelated one-electron transition, it should correspond to the interband minimum, and the phase angle is further restricted to the range $0<\phi<90°$). The phase angles observed in this work correspond to mixtures of a 2D maximum and a saddle point, as was reported for $Cd_xHg_{1-x}Te$,[43] $Cd_xMn_{1-x}Te$,[44] and $Al_xGa_{1-x}As$.[39] If this phase angle ϕ is small, it can be used as a phenomenological measure of excitonic effects in the line shapes.[70,83] However, even in the case of larger ϕ, the same interpretation has been applied.[39,44,84] If ϕ is a measure of the excitonic effects, the dependence of ϕ on x shown in Fig. 10 is reasonable: they should become smaller with increasing disorder and thus reach a minimum for $x\sim0.5$. Again without the linear background, the fitted quadratic curves have their exact minimum at $x=0.5$, showing the same symmetric behavior as $\Gamma(x)$.

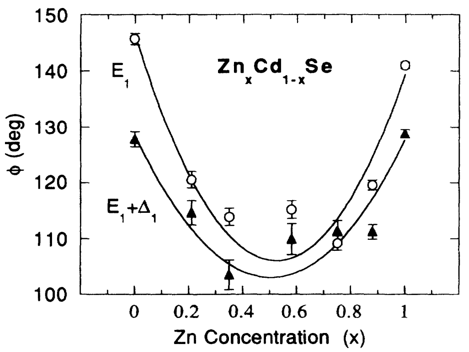

FIG. 10. Dependence on concentration x of the excitonic parameters defined in Eq. (2) for $Zn_xCd_{1-x}Se$. Solid lines are fits to the quadratic x dependence.

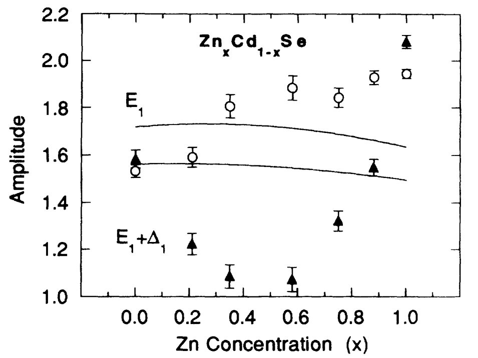

FIG. 11. Dependence on composition x of the amplitude parameters defined in Eq. (2) for $Zn_xCd_{1-x}Se$. Solid lines represent the calculated E_1 and $E_1+\Delta_1$ strengths according to Eq. (6).

Finally the amplitudes of the E_1 (A_{E_1}) and $E_1+\Delta_1$ ($A_{E_1+\Delta_1}$) transitions are shown in Fig. 11. While A_{E_1} increases fairly linearly with x, $A_{E_1+\Delta_1}$ has its minimum at $x\sim0.5$. The amplitudes for 2D E_1 and $E_1+\Delta_1$ transitions can be calculated in the one-electron approximation with[85]

$$\begin{aligned} A_{E_1} &\approx 44(E_1+\Delta_1/3)/a_0E_1^2 , \\ A_{E_1+\Delta_1} &\approx 44(E_1+2\Delta_1/3)/a_0(E_1+\Delta_1)^2 , \end{aligned} \tag{6}$$

where a_0 is the lattice constant in Å, and the energies are in eV. The calculated amplitudes according to Eq. (6) (shown in Fig. 10 as solid lines) do not explain our data. This result has been also found in $Al_xGa_{1-x}As$,[39] and the discrepancy was attributed to excitonic interaction. The result of this analysis is consistent with the fact that the one-electron picture without electron-hole interaction in the calculated ε_2 spectrum of CdSe could not explain our data in Sec. III A.

IV. CONCLUSIONS

We have measured the dielectric function of zinc-blende $Zn_xCd_{1-x}Se$ alloy films ($0\leq x\leq1$) grown on GaAs(001) substrates by means of spectroscopic ellipsometry in the 1.5–6.0 eV region. A chemical etching procedure to remove the natural oxide overlayer was applied to obtain the best dielectric response of these alloys.

The band structure of CdSe with spin-orbit splitting was calculated by the nonlocal pseudopotential method with special emphasis on identifying the $E_2(X_7^v \rightarrow X_6^c)$ (~ 6.0 eV) transition. The calculated dielectric function obtained from the band structure without many-body effects showed a large discrepancy with data. Including electron-hole interactions by means of the contact excitonic potential with adjustable strength gave good agreement with the measured spectrum. This indicates the importance of the excitonic effect even though the exciton binding energy for the Γ point is only about 8 meV, which is must less than $k_B T$ at room temperature. The critical-point parameter study for E_1 and $E_1+\Delta_1$ transitions was done from a fit to second-derivative spectra of several $\mathrm{Zn}_x\mathrm{Cd}_{1-x}\mathrm{Se}$ alloys. The concentration-dependent energies, linewidth, and excitonic phase angles obtained were fit to quadratic equations, and the results were reported. The observed nonlinear dependence of the spin-split gap Δ_1 on alloy concentration was explained well as a disorder-induced effect.[77] The line broadenings and phase angles showed symmetric behavior, having their extremum at $x=0.5$, whereas the amplitudes did not follow the estimated values according to the one-electron approximation, consistent with many-body effect observed in the CdSe spectrum.

ACKNOWLEDGMENTS

Y.D.K., M.V.K., and Y.C.C. were supported by the Materials Research Laboratory through NSF/MRL Grant No. DMR 89-20538, S.F.R. by ONR Grant No. N00014-90-J-1267, and University of Notre Dame work was supported by ONR Grant No. N00014-90-J-1782 and NSF/MRG Grant No. DMR 92-21390.

---

[*] Present address: Department of Physics, Pennsylvania State University.

[1] See for instance, *Physics and Chemistry of II-VI Semiconducting Compounds* (North-Holland, Amsterdam, 1967).

[2] R. G. Wheeler and J. O. Dimmock, Phys. Rev. **125**, 1805 (1962).

[3] M. Cardona, Phys. Rev. **129**, 1068 (1963).

[4] M. Cardona and G. Harbeke, Phys. Rev. **137**, A1467 (1965).

[5] M. Cardona, K. L. Shaklee, and F. H. Pollak, Phys. Rev. **154**, 696 (1967).

[6] J. L. Freeouf, Phys. Rev. B **7**, 3810 (1973).

[7] H. Lange and I. A. Iliev, Phys. Status Solidi B **84**, 569 (1977).

[8] J. Voigt, F. Spiegelberg, and M. Senoner, Phys. Status Solidi B **91**, 189 (1979).

[9] S. F. Terekhova, N. A. Onishchenko, O. N. Talenskii, and S. A. Pendur, Phys. Status Solidi B **91**, 207 (1979).

[10] R. B. Parsons, W. Wardzynski, and A. D. Yoffe, Proc. R. Soc. London, Ser. A **262**, 120 (1961).

[11] V. V. Sobolev, V. I. Donetskikh, and E. F. Zagainov, Fiz. Tekh. Poluprovodn. **12**, 1089 (1978) [Sov. Phys. Semicond. **12**, 646 (1978)].

[12] I. A. Iliev, M. N. Iliev, and H. Lange, Phys. Status Solidi B **69**, K157 (1975).

[13] T. K. Bergstresser and M. L. Cohen, Phys. Rev. **164**, 1069 (1967).

[14] A. Kobayashi, O. F. Sankey, S. M. Volz, and J. D. Dow, Phys. Rev. B **28**, 935 (1983).

[15] M. Z. Huang and W. Y. Ching, J. Phys. Chem. Solids **46**, 977 (1985).

[16] H. Jeon, J. Ding, A. V. Nurmikko, H. Luo, N. Samarth, J. K. Furdyna, W. A. Bonner, and R. E. Nahory, Appl. Phys. Lett. **57**, 2413 (1990).

[17] M. A. Haase, J. Qiu, J. M. DePuydt, and H. Cheng, Appl. Phys. Lett. **59**, 1272 (1991).

[18] H. Luo, N. Samarth, J. K. Furdyna, H. Jeon, J. Ding, N. Pelekanos, and A. V. Nurmikko, in *Materials for Optical Information Processing*, edited by C. Warde, J. Stamatoff, and W. Wang, MRS Symposia Proceedings No. 228 (Materials Research Society, Pittsburgh, 1992), p. 301.

[19] S. Logothetidis, M. Cardona, P. Lautenschlager, and M. Garriga, Phys. Rev. B **34**, 2458 (1986).

[20] C. Gourdon and P. Lavallard, Phys. Rev. B **31**, 6654 (1985).

[21] S. Adachi, J. Appl. Phys. **68**, 1192 (1990).

[22] N. Samarth, H. Luo, J. K. Furdyna, R. G. Alonso, Y. R. Lee, A. K. Ramdas, S. B. Qadri, and N. Otsuka, Appl. Phys. Lett. **56**, 1163 (1990).

[23] N. Samarth, H. Luo, J. K. Furdyna, S. B. Qadri, Y. R. Lee, R. G. Alonso, E. K. Suh, A. K. Ramdas, and N. Otsuka, Surf. Sci. **228**, 226 (1990).

[24] P. Juza, H. Zajicek, H. Sitter, M. Helm, W. Faschinger, and K. Lischka, Appl. Phys. Lett. **61**, 3133 (1992).

[25] J. A. V. Vechten and T. K. Bergstresser, Phys. Rev. B **1**, 3351 (1970).

[26] D. Stroud, Phys. Rev. B **5**, 3366 (1972).

[27] K. C. Hass, H. Ehrenreich, and B. Velicky, Phys. Rev. B **27**, 1088 (1983).

[28] D. J. Chadi, Phys. Rev. B **16**, 790 (1977).

[29] O. Berolo, J. Woolley, and J. A. V. Vechten, Phys. Rev. B **8**, 3794 (1973).

[30] D. E. Aspnes, in *Optical Properties of Solids: New Developments,* edited by B. O. Seraphin (North-Holland, Amsterdam, 1976), p. 799.

[31] D. E. Aspnes and A. A. Studna, Phys. Rev. B **27**, 985 (1983).

[32] P. Lautenschlager, M. Garriga, L. Viña, and M. Cardona, Phys. Rev. B **36**, 4821 (1987).

[33] L. Viña, S. Logothetidis, and M. Cardona, Phys. Rev. B **30**, 1979 (1984).

[34] S. M. Kelso, D. E. Aspnes, M. A. Pollack, and R. E. Nahory, Phys. Rev. B **26**, 6669 (1982).

[35] D. E. Aspnes, S. M. Kelso, R. A. Logan, and R. Bhat, J. Appl. Phys. **60**, 754 (1986).

[36] P. Lautenschlager, M. Garriga, S. Logothetidis, and M. Cardona, Phys. Rev. B **35**, 9174 (1987).

[37] P. Lautenschlager, M. Garriga, and M. Cardona, Phys. Rev. B **36**, 4813 (1987).

[38] S. Zollner, C. Lin, E. Schönherr, A. Böhringer, and M. Cardona, J. Appl. Phys. **66**, 383 (1989).

[39] S. Logothetidis, M. Cardona, and M. Garriga, Phys. Rev. B **43**, 11 950 (1991).

[40] H. Yao, P. G. Snyder, and J. A. Woollam, J. Appl. Phys. **70**, 3261 (1991).

[41] A. R. Heyd, R. W. Collins, K. Vedam, S. S. Bose, and D. L. Miller, Appl. Phys. Lett. **60**, 2776 (1992).

[42] H. Arwin and D. E. Aspnes, J. Vac. Sci. Technol. A **2**, 1316

(1984).

[43] L. Viña, C. Umbach, M. Cardona, and L. Vodopyanov, Phys. Rev. B **29**, 6752 (1984).

[44] P. Lautenschlager, S. Logothetidis, L. Viña, and M. Cardona, Phys. Rev. B **32**, 3811 (1985).

[45] K. Kumazaki, L. Viña, C. Umbach, and M. Cardona, Phys. Status Solidi B **156**, 371 (1989).

[46] S. Adachi and T. Taguchi, Phys. Rev. B **43**, 9569 (1991).

[47] Y. D. Kim, S. L. Cooper, M. V. Klein, and B. T. Jonker, Appl. Phys. Lett. **62**, 2387 (1993).

[48] A. S. Nasibov, Y. V. Korostelin, P. V. Shapin, L. G. Suslina, D. L. Fedorov, and L. S. Matkov, Solid State Commun. **71**, 867 (1989).

[49] H. Luo, N. Samarth, F. C. Zhang, A. Pareek, M. Dobrowolska, J. K. Furdyna, K. Mahalingam, N. Otsuka, W. C. Chou, A. Petrou, and S. B. Qadri, Appl. Phys. Lett. **58**, 1783 (1991).

[50] N. Samarth, H. Luo, J. K. Furdyna, S. B. Qadri, Y. R. Lee, A. K. Ramdas, and N. Otsuka, J. Electron. Mater. **19**, 543 (1990).

[51] D. E. Aspnes, Opt. Commun. **8**, 222 (1973).

[52] D. E. Aspnes and A. A. Studna, Appl. Opt. **14**, 220 (1975).

[53] R. M. A. Azzam and N. M. Bashara, *Ellipsometry and Polarized Light* (North-Holland, Amsterdam, 1977).

[54] W. Kern and C. A. Deckert, in *Thin Film Processes*, edited by J. L. Vossen and W. Kern (Academic, New York, 1978), Chap. 5-1.

[55] D. E. Aspnes and A. A. Studna, Rev. Sci. Instrum. **49**, 291 (1978).

[56] J. R. Chelikowsky and M. L. Cohen, Phys. Rev. B **14**, 556 (1976).

[57] D. J. Stukel, R. N. Euwema, T. C. Collins, F. Herman, and R. L. Kortum, Phys. Rev. **179**, 740 (1968).

[58] W. H. Duan, B. L. Gu, and J. L. Zhu, Acta Phys. Sin. **39**, 437 (1989).

[59] J. L. Birman, Phys. Rev. **115**, 1493 (1959).

[60] R. Ludeke and W. Paul, in *II-VI Semiconducting Compounds International Conference*, edited by D. G. Thomas (Benjamin, New York, 1967), p. 123.

[61] F. Bassani and C. P. Parravicini, *Electronic States and Optical Properties in Solids* (Pergamon, New York, 1975).

[62] G. F. Koster and J. C. Slater, Phys. Rev. **96**, 1208 (1954).

[63] B. Velicky and J. Sak, Phys. Status Solidi **16**, 147 (1966).

[64] J. E. Rowe and D. E. Aspnes, Phys. Rev. Lett. **25**, 162 (1970).

[65] Y. C. Chang and R. B. James, Phys. Rev. B **46**, 15 040 (1992).

[66] R. M. Martin, J. A. V. Vechten, J. E. Rowe, and D. E. Aspnes, Phys. Rev. B **6**, 2500 (1972).

[67] I. Broser, R. Broser, and A. Hoffman, in *Physics of II-VI and I-VII Compounds, Semimagnetic Semiconductors*, edited by O. Madelung, Landolt-Börnstein, New Series, Group III, Vol. 17, Pt. b (Springer, Berlin, 1982), p. 202.

[68] D. E. Aspnes, J. Vac. Sci. Technol. **17**, 1057 (1980).

[69] A. Savitzky and J. E. Gollay, Anal. Chem. **36**, 1627 (1974).

[70] M. Cardona, in *Modulation Spectroscopy*, edited by F. Seitz, D. Turnbull, and H. Ehrenreich, *Solid State Physics* Suppl. 11 (Academic, New York, 1969).

[71] D. E. Aspnes, in *Handbook on Semiconductors*, edited by M. Balkanski (North-Holland, Amsterdam, 1980), Vol. 2, p. 109.

[72] M. Cardona, Phys. Rev. **129**, 69 (1963).

[73] A. G. Thompson, M. Cardona, K. L. Shaklee, and J. C. Woolley, Phys. Rev. **146**, 601 (1966).

[74] E. W. Williams and V. Rehn, Phys. Rev. Lett. **27**, 798 (1968).

[75] C. Alibert, G. Bordure, A. Laugier, and J. Chevalier, Phys. Rev. B **6**, 1301 (1972).

[76] P. Parayanthal and F. Pollak, Phys. Rev. B **28**, 3632 (1983).

[77] J. A. V. Vechten, O. Berolo, and J. C. Woolley, Phys. Rev. Lett. **29**, 1400 (1972).

[78] *Table of Periodic Properties of the Elements* (Sargent-Welch, Skokie, 1992).

[79] N. W. Ashcroft and N. D. Mermin, *Solid State Physics* (Saunders College, Philadelphia, 1976), p. 5.

[80] O. Goede, L. John, and D. Hennig, Phys. Status Solidi B **89**, K183 (1978).

[81] E. F. Schubert, E. O. Gobel, Y. Horikoshi, K. Ploog, and H. J. Queisser, Phys. Rev. B **30**, 813 (1984).

[82] Y. Toyozawa, M. Inoue, T. Inui, M. Okazaki, and E. Hanamura, J. Phys. Soc. Jpn. Suppl. **21**, 133 (1966).

[83] Y. Toyozawa, M. Inoue, T. Inui, M. Okazaki, and E. Hanamura, J. Phys. Soc. Jpn. Suppl. **22**, 1337 (1967).

[84] L. Viña and M. Cardona, Phys. Rev. B **29**, 6739 (1984).

[85] M. Cardona, in *Light Scattering in Solids II*, edited by M. Cardona and G. Güntherodt (Springer-Verlag, Berlin, 1982), p. 119.